

On the relationship between Ural blocking and Arctic-midlatitude thermal gradient

Marco Cadau¹, Gabriele Messori^{2,3,4}, Marco Gaetani¹, Giorgia Fosser¹, Simona Bordini⁵, Roberto Buizza⁶, Gianmaria Sannino⁷

¹Scuola Universitaria Superiore IUSS, Pavia, Italy

²Department of Earth Sciences, Uppsala University, Uppsala, Sweden

³Swedish Centre for Impacts of Climate Extremes (climes), Uppsala University, Uppsala, Sweden

⁴Department of Meteorology and Bolin Centre for Climate Research, Stockholm University, Stockholm,

Sweden

⁵Department of Civil, Environmental and Mechanical Engineering (DICAM), University of Trento,

Trento, Italy

⁶Interdisciplinary Research Center on Sustainability and Climate, Scuola Superiore Sant'Anna, Pisa, Italy

⁷Italian National Agency for New Technologies, Energy and the Environment (ENEA), Rome, Italy

Key Points:

- Ural Blocking can be characterised by strong Arctic-midlatitude thermal gradient
- Co-occurrence of Ural blocking with blocking over Greenland and Chukotka and Urals leads to strong Arctic-midlatitude thermal gradient
- Blocking displacement north of the Ural region leads to weak Arctic-midlatitude thermal gradient

Corresponding author: Marco Cadau, marco.cadau@iusspavia.it

Abstract

[In this study, the relationship between the interannual variability of Arctic-midlatitude thermal gradient (AMG) and the winter atmospheric blocking frequency in the Ural region (UBF) is investigated in the ERA5 reanalysis product from 1940 to 2023. In particular, the paper focuses on the large-scale atmospheric circulation patterns associated with high UBF concomitant to weak AMG and vice versa, revisiting the more common and documented relationship connecting intense Ural blocking activity to strong AMG. Results show that displacements of the atmospheric blocking from the Ural region towards the Arctic lead to anomalous southerly thermal advections at polar latitudes and stronger AMG. On the other hand, high blocking frequency co-occurring in the Ural, Greenland and Chukotka regions lead to weaker AMG by limiting northward heat advections towards the Arctic region. These findings highlight a more complex picture of the role of subpolar atmospheric circulation in controlling the AMG.]

Plain Language Summary

[Blocking of the mean atmospheric flow over the Ural region is an important feature of high-latitude weather affecting climate variability in the Arctic. In general, the occurrence of the Ural blocking is associated with warm anomalies in the Arctic, leading to a decrease in the thermal difference between polar and mid latitudes, while reduced blocking activity is generally associated with a larger difference in temperature. This article examines the role of Ural blocking in controlling the Arctic-midlatitudes thermal difference by analyzing unconventional situations. In particular, we find that blocking occurring north of the Ural region leads to a warmer Arctic and a reduced temperature difference, while the co-occurrence of blocking over the Urals, Greenland and Chukotka blocking inhibits the heat transport from mid towards polar latitudes, increasing the thermal difference. These findings contribute to shed light on the mechanisms controlling the Arctic amplification, that is the faster warming of the Arctic region with respect to the global warming.]

1 Introduction

Atmospheric blocking, namely a disruption and/or a deceleration of the mean westerly circumpolar flow, is one of the most important features of the large-scale atmospheric circulation at mid-high latitudes (Davini et al., 2012). Blocking events are associated with anomalous anticyclonic conditions that persist from several days to weeks (Kwon et al., 2020; AMS, American Meteorological Society, 2012; Wazneh et al., 2021). This long persistence is associated with quasi-stationarity (Crocini-Maspoli et al., 2007) and self-sustaining or self-preserving mechanisms (Kautz et al., 2022).

During the winter season, the establishment of blocking can lead to large-scale temperature anomalies over the continents in the Northern Hemisphere (NH) and in the Arctic region (Kautz et al., 2022). Winter atmospheric blocking activity in the NH is most frequent in the Bering Strait region, over Greenland and in the Euro-Atlantic sector (1a) (Davini et al., 2012; Woollings et al., 2018; Davini et al., 2021; Hwang et al., 2022). The latter is the most spatially extended blocking region, extending all the way to the Urals. Although Ural blocking (UB) displays a comparatively modest occurrence frequency, it has important repercussions, both locally and in the broader high-latitude Eurasian region. These include affecting sea-ice formation and persistence - especially over the Barents-Kara Seas (Chen et al., 2018; Cho & Kim, 2021) - and influencing Eurasian cooling (Tyrlis et al., 2020; Kim et al., 2022) and Arctic warming (D. Luo, Xiao, Yao, et al., 2016; Yao et al., 2017a). The role of Ural Blocking in inducing these anomalies is modulated by other large-scale patterns, such as the North Atlantic Oscillation and the configuration of the North Atlantic jet (D. Luo, Xiao, Yao, et al., 2016; D. Luo, Xiao, Diao, et al., 2016),

70 but also by the atmospheric background conditions such as the mean state and vertical
71 shear of the westerly flow (Yao et al., 2017b; D. Luo et al., 2017).
72 The literature highlights a positive correlation between UB and Arctic temperatures and
73 a negative correlation between UB and Siberian temperatures (D. Luo, Xiao, Yao, et al.,
74 2016; Tyrlis et al., 2020; Papritz, 2020). UB thus acts to reduce the hemispheric-scale
75 temperature gradient. The role of UB in favouring a warmer Arctic has received con-
76 siderable attention, as one of the several mechanisms potentially modulating Arctic Am-
77 plification (AA) (Tyrlis et al., 2020; Cho & Kim, 2021). AA refers to the observed faster-
78 than-global-average warming of the Arctic, which is leading to a decreased thermal gra-
79 dient between the northern high and mid latitudes (hereafter referred to as Arctic-midlatitude
80 thermal gradient, or AMG) on multidecadal timescales. AA is induced by multiple fac-
81 tors, including (but not limited to) local longwave and shortwave feedbacks, such as lapse
82 rate and sea-ice related feedbacks (Screen & Simmonds, 2010; England et al., 2021), as
83 well as remote influences by poleward energy transport (Graversen & Burtu, 2016; Pre-
84 vidi et al., 2021). The AMG plays an important role in large-scale climate dynamics, by
85 affecting mid-latitude stormtracks (Shaw et al., 2016), meridional moist and dry static
86 energy transports, the orientation and intensity of the jetstream, sea-ice cover and more
87 (Deser et al., 2015; Screen & Francis, 2016).
88 Notwithstanding the extensive research on AMG and UB, the relationship between the
89 two remains not completely understood. In particular, comparatively little attention has
90 been dedicated to the relationship between the AMG and blocking activity at interan-
91 nual timescales. This study aims to shed light on this relationship, and verify the extent
92 to which deviations can occur from the expected decreased (increased) gradient in the
93 presence of more (less) UB

94 2 Data and methods

95 2.1 Data and significance testing

96 We use geopotential height at 500 hPa (z_{500}), air temperature at 1000hPa (t_{1000}),
97 meridional wind at 850hPa (v_{850}), the vertical integral of northward total heat flux (HEATF)
98 and of the divergence of thermal energy flux (THERMF) from the ERA5 reanalysis prod-
99 uct of the European Centre for Medium-Range Weather Forecasts (Hersbach et al., 2020).
100 All the data are analysed at a $1^\circ \times 1^\circ$ horizontal resolution (remapped from data at a quar-
101 ter of a degree resolution). Since we focus on large-scale circulation features across the
102 NH, we deem the lower resolution not to affect our analysis. The analysis is performed
103 on 83 boreal winters (December, January and February, DJF), corresponding to 249 months,
104 from December 1940 to February 2023.
105 Linear correlations are computed using the Pearson correlation coefficient, and consid-
106 ered significant when above the 95% confidence level. The significance of climate vari-
107 ables anomalies is determined using Montecarlo sampling (Kroese et al., 2014) with 5000
108 iterations, at the 2.5% one-sided significance level.

109 2.2 Blocking detection

110 We implement a two-dimensional extension of the Tibaldi and Molteni (Tibaldi &
111 Molteni, 1990) blocking index, introduced by Scherrer et al. (Scherrer et al., 2005). This
112 is amongst the most widely used blocking indices, and is based on the reversal of the merid-
113 ional gradient of the 500hPa geopotential height (Z_{500}). At each grid point, we compute:

$$GHGN = \frac{(Z_{500}(\lambda, \phi + \delta)) - Z_{500}(\lambda, \phi)}{\delta} \quad (1)$$

$$GHGS = \frac{(Z_{500}(\lambda, \phi)) - Z_{500}(\lambda, \phi - \delta)}{\delta} \quad (2)$$

$$GHGS_2 = \frac{(Z_{500}(\lambda, \phi - \delta)) - Z_{500}(\lambda, \phi - 2\delta)}{\delta} \quad (3)$$

116 with λ and ϕ indicating longitude and latitude, respectively, and $\delta = 15^\circ$.
 117 In order to consider a grid point as blocked, three conditions must be satisfied:

$$GHGN < -10 \frac{m}{^\circ latitude} \quad (4)$$

$$GHGS > 0 \frac{m}{^\circ latitude} \quad (5)$$

$$GHGS_2 < -5 \frac{m}{^\circ latitude} \quad (6)$$

120 The first two conditions imply that a blocked area must display a westerly flow on its
 121 poleward side (4) and an easterly flow on its equatorward side (5) (Tyrlis et al., 2021).
 122 4 excludes situations when the midlatitude jet is displaced but not blocked, which might
 123 be otherwise classified as blocking (Tibaldi & Molteni, 1990). Lastly, 6 excludes cut-off
 124 lows and subtropical features (Davini et al., 2012; Woollings et al., 2018).

125 In this study, we only consider instantaneous blocking (IB) (Davini et al., 2012; Davini
 126 & D’Andrea, 2020), namely not implementing any temporal persistence condition or spa-
 127 tial extent constraint. We define UB as IB occurring in the Ural region [54°-64°N, 48°-
 128 67°E] (highlighted in yellow in Figure 1a). A Ural Blocking Index (UBI) is then calcu-
 129 lated as follows. We first determine the monthly blocking frequency at each gridpoint
 130 as the percentage of days with presence of blocking over the total of the days of the month.
 131 We next compute an area-weighted spatial average, across all gridpoints within the se-
 132 lected Ural region.

133 2.3 Arctic-midlatitudes thermal gradient

134 The AMG definition is based on the 1000hPa temperature anomalies, following Fran-
 135 cis and Vavrus, 2015 and Davy et al., 2018 (Francis & Vavrus, 2015; Davy et al., 2018).
 136 We subtract the monthly temperature anomaly of the [30-60°N] band from the correspond-
 137 ing anomaly of the [70-90°N] band. The anomalies are computed with respect to the cor-
 138 responding monthly long term climatology. For example, the t1000 anomaly for Decem-
 139 ber 1940 is given by the difference in temperature, previously averaged over the selected
 140 latitude band, between December 1940 and the areal mean climatological temperature
 141 for all Decembers over the 1940-2022 period. Thus, high values of the AMG index are
 142 associated with a lower than average meridional gradient, and viceversa.

143 The resulting AMG timeseries (Figure 1b) includes both high frequency and low frequency
 144 variability. The long-term increasing trend is the footprint of AA, and corresponds to
 145 a faster warming of the high latitude band compared to the midlatitudes. A visual in-
 146 spection nonetheless suggests that the increasing trend is non-monotonic. In order to iso-
 147 late the high-frequency (HF) component of the signal, the low frequency component, es-
 148 timated by applying a 6th grade polynomial fit, is subtracted from the AMG time se-
 149 ries. The HF component is isolated from each month (D, J and F) separately. The re-
 150 sulting AMG-HF is displayed in the supplementary material (Figure ??). The appli-
 151 cation of a low-pass filter with a cut-off frequency of 8 years leads to similar results (not
 152 shown), indicating that the definition of the HF component of the AMG is not sensitive
 153 to the filtering method.

154 We interpret AMG-HF as illustrating the AA’s interannual variability.

155 3 Results

156 In agreement with previous research, we find a significant positive correlation be-
 157 tween UB frequency and AMG (Figure 1c). Indeed, the Urals are the blocking region
 158 displaying the strongest absolute correlation values. Thus, Ural blockings are more fre-
 159 quent in months characterised by a positive AMG index (associated to a reduced merid-
 160 ional thermal gradient), and viceversa.

161 A similar, but stronger, signal is found when the long-term variability is removed
 162 to AMG (Figure 1d). This suggests that the UB relationship is stronger at the interan-
 163 nual time scale. Specifically, the correlation coefficient spatially averaged over the Ural

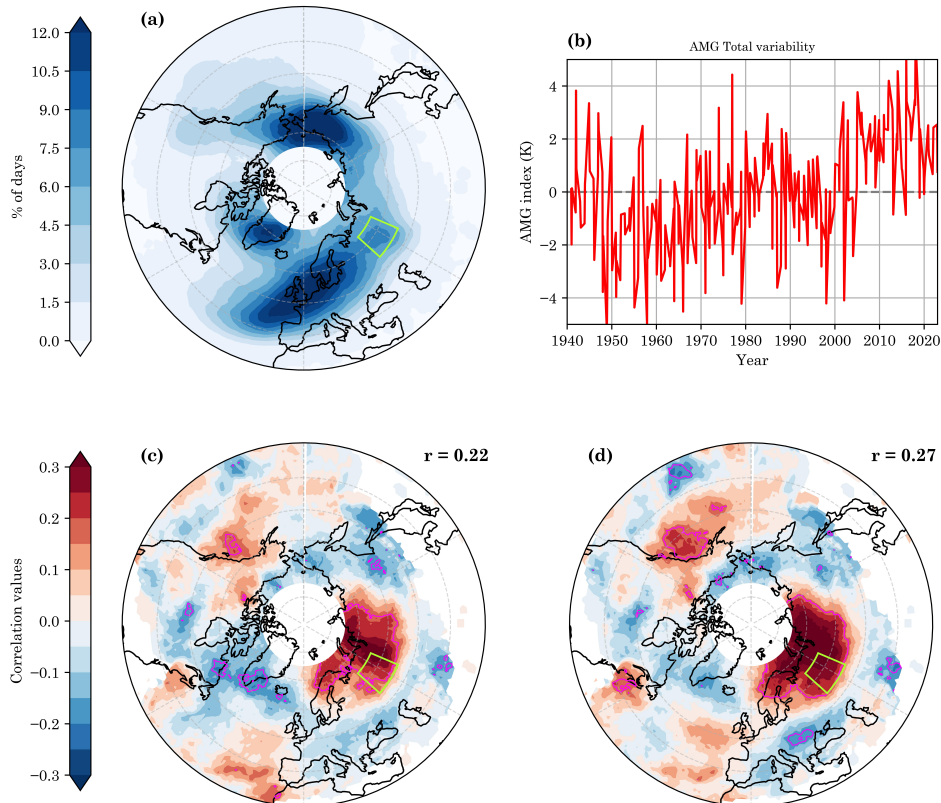


Figure 1. (a) DJF Climatology of instantaneous blocking (IB) frequency in the [30-75°N] band. The Ural region is highlighted by the light green box. (b) Arctic-midlatitudes thermal gradient (AMG), DJF monthly means from 1940 to 2022. Note that timeseries only displays DJF values for each year. Pearson correlation maps between monthly timeseries of IB and AMG: (c) unfiltered and (d) high frequency. Magenta lines mark significance at the 5% level. In panels (c) and (d), the correlation coefficients spatially averaged over the Ural region (light green box), with their p-values, are displayed. Correlation coefficients spatial averages are statistically significant at the 1% level.

164 region expresses about 7.2% of the shared variability for the AMG-HF, against less than
 165 5% for the raw AMG index. We thus focus on the relationship between AMG-HF and
 166 UBI.

167 As expected from the correlation map, the months with high Ural blocking activity are
 168 likely to be months with large AMG-HF index values, and the converse. However, there
 169 are also relatively numerous cases where high Ural blocking activity coincides with a low
 170 AMG-HF index and viceversa. This is not entirely unexpected, as the linear correlation
 171 explains a relatively small fraction of the covariance between the two variables.

172 To better characterize these "unconventional" cases, in Figure 2, we classify all the 249
 173 DJF months we analyse according to their joint AMG-HF and instantaneous Ural Block-
 174 ing values. We select four subsets of months for further analysis: two are the "conven-
 175 tional" cases of high (low) AMG-HF index values and strong (weak) UBI, including 36
 176 (51) months. We hereafter name this case SS (WW), from Strong AMG-HF-Strong UBI
 177 (WW, from Weak AMG-HF-Weak UBI). Part of the remaining months fall into the un-
 178 conventional cases of low (high) AMG-HF index and strong (weak) Ural blocking, in-

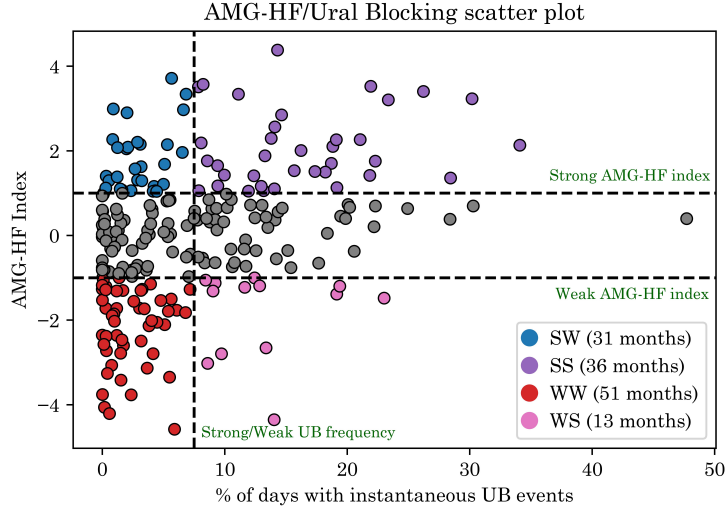


Figure 2. Scatterplot of monthly UBI and AMG-HF index. Blue dots display anomalously positive AMG-HF index values associated with low UBI (strong AMG-HF index and weak UBI, SW). Purple dots display anomalously high AMG-HF index values associated with high UBI (strong AMG-HF index and strong UBI, SS). Red dots display anomalously negative AMG-HF index values associated with low UBI (weak AMG-HF index and weak UBI, WW). Pink dots display anomalously negative AMG-HF index values associated with high UBI (weak AMG-HF index and strong UBI, SS). The sample sizes of the WW, WS, SW and SS are indicated in the legend.

179 cluding 13 (31) months, hereafter named WS (SW). Note that high (low) values of the
 180 AMG-HF index are associated with a gradient weaker (stronger) than usual.
 181 To define these four sets of months, we use thresholds values of ± 1 K for the AMG-HF
 182 index, approximately corresponding to the 25th and 75th percentiles of the index. We
 183 further use a cutoff of 7.5% blocking frequency to separate strong and weak UBI, approx-
 184 imately corresponding to the 61st percentile of the UBI distribution.

185 To shed light on the dynamical features of the AMG-UB relationship at the inter-
 186 annual time scale, the large-scale atmospheric circulation patterns associated with the
 187 identified classes of events are analysed.
 188 When both the AMG-HF index and UBI are lower than usual (WW case) we observe
 189 a significant decrease in frequency of IB from Scandinavia through Eastern Europe and
 190 across Siberia (Figure 3a). Hence, the observed decreased blocking frequency signal is
 191 not limited to Urals, but extended to a much broader region. An analogous decrease is
 192 observed in the Gulf of Alaska and, at the same time, blocking frequency increases in
 193 Southeastern Europe. Z500 anomalies reflect the blocking anomalies (Figure 3a). The
 194 t1000 patterns are characterized by widespread negative anomalies over the Arctic re-
 195 gion, and an extended positive anomaly over Eurasia (Figure 3b). The decreased UB fre-
 196 quency further shows its signature in meridional 850 hPa wind (Figure 3c) which dis-
 197 plays a cyclonic anomaly over the Ural region. A positive anomaly over Northern Canada
 198 is observed, as well as a negative v850 anomaly south of Greenland and in the North At-
 199 lantic region south of the Arctic ocean. The latter suggests a weakened advection of warm
 200 and moist airmasses towards the polar latitudes from the North Atlantic sector, contrib-
 201 uting to the higher-than-average meridional temperature gradient. This interpretation is
 202 supported by the HEATF anomalies (Figure ??a), strongly resembling the spatial pat-
 203 tern of v850. Finally, the area-weighted spatial average of the THERMF anomalies over

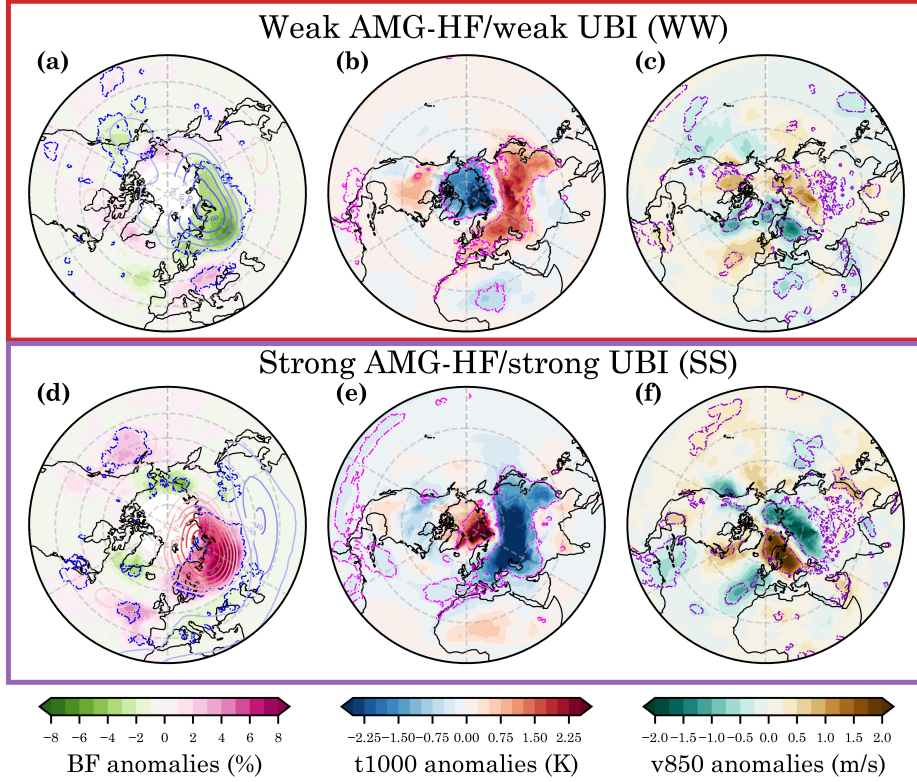


Figure 3. Compound climate anomalies for the four sets of months defined in 3 and in Figure 2: low AMG-HF index/weak UB (red), high AMG-HF index/strong UB (purple), high AMG-HF index/weak UB (blue) and low AMG-HF index/strong UB (pink). Anomalies are shown for the following variables: (a), and (d) Blocking Frequency (BF); (b) and (e) 1000hPa temperature; (c) and (f) 850hPa meridional wind. Dashed contours denote significant anomalies at the 95% confidence level, determined using Monte Carlo sampling with 5000 iterations. blue-to-red scale contours on BF anomalies represent 500hPa geopotential anomalies for the same time frame.

204 the Arctic region (defined as for the AMG metric, as the [70-90°N] band) is positive (8.85
 205 W/m) in the WW case: positive values of this indicator are associated with a net diver-
 206 gence of the thermal energy flux over the Arctic. gradient.

207 When both AMG-HF index and Ural Blocking activity are higher than usual (SS),
 208 the anomalies are approximately symmetric to the WW case (Figure 3d-f). The main
 209 differences are a significant negative anomaly in blocking frequency over southern Green-
 210 land and a positive anomaly over the North Atlantic. The THERMF pattern is also con-
 211 sistent with the previous interpretation of the WW case, since the Arctic THERMF spa-
 212 tial average is statistically significantly negative at -18.76 W/m, suggesting a net con-
 213 vergence of thermal energy flux in the Arctic.

214 We next consider the two unconventional cases in the relationship between Ural Block-
 215 ing and AMG. The SW case displays negative IB frequency anomalies over the Urals (Fig-
 216 ure 4a). However, unlike the WW case (Figure 3a), the region of negative anomalies is
 217 much more spatially confined. A positive signal over the Barents-Kara seas suggest that
 218 the weakening of the UB reflects a northward shift of the blocking region, which cannot
 219 be captured by our blocking metric, defined south of 75°N. Nevertheless, the hypothe-
 220 sis of a displacement of the blocking regions is supported by the positive z500 anoma-
 221 lies seen over the Arctic Ocean (Figure 4a). T1000 anomalies are strongly positive over

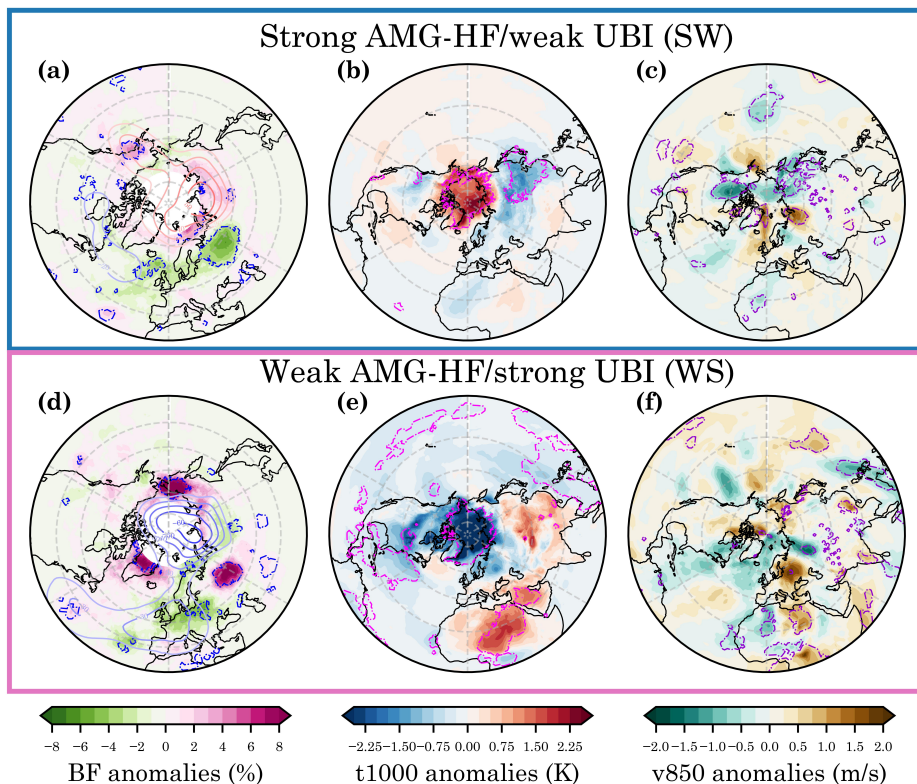


Figure 4. Same as in 3, but for (a-c) SW and (d-f) WS.

222 the Arctic. They are however widespread across the Arctic basin, unlike for the SS case,
 223 where the strongest positive anomalies were concentrated in the Barents-Kara seas re-
 224 gion (cf. Figure 4b, Figure 3e). The negative anomalies over Eurasia are weak, and con-
 225 fined to Eastern Siberia. V850 anomalies show a cyclonic pattern anomaly over Siberia,
 226 a strong negative anomaly over central Canada and positive anomalies in the North At-
 227 lantic sector. This latter, along with the HEATF anomalies pattern (Figure ??a) sug-
 228 gests enhanced advection of midlatitude airmasses towards the high latitudes.
 229 The WS case shows anomalies which only partly mirror those for the SW case. The posi-
 230 tive UBI anomaly is intense, but geographically very localized (Figure 4d). Strong posi-
 231 tive blocking anomalies are also found in correspondence with the climatological max-
 232 ima in Greenland and the Bering Strait. These anomalies exceed 6%, namely over 50%
 233 of the climatological values (Figure 1a) of about 8-12% of blocking days. The Z500 anoma-
 234 lies are strongly negative in the Arctic basin, but unlike the SW case, do not form an
 235 Arctic-mid latitude dipole (Figure 4d). The t1000 pattern displays a colder-than-average
 236 Arctic, similar to the WW case, yet with stronger and more widespread negative anoma-
 237 lies (cf. Figure 3b, Figure 4e). Moreover, there is only a weak warming signal over Eur-
 238 asia, with the cold anomalies extending from the Arctic into Scandinavia, Western Rus-
 239 sia and northern North America. Both positive and negative temperature anomalies are
 240 found across the lower midlatitudes: in particular, a significant and positive tempera-
 241 ture anomaly is present over central Sahara and over the Arabian desert. Finally, the
 242 v850 anomalies do not display relevant significant signals, apart from the anticyclonic
 243 pattern over the Ural region, albeit less marked than for SS (cf. Figure 4f, Figure 3f).
 244 Although not significant, a negative anomaly over the North Atlantic might suggest, as
 245 in the SW case, a weakened heat and moisture transport towards the polar latitudes, as
 246 also supported by the HEATF anomalies showing again a strong association between merid-

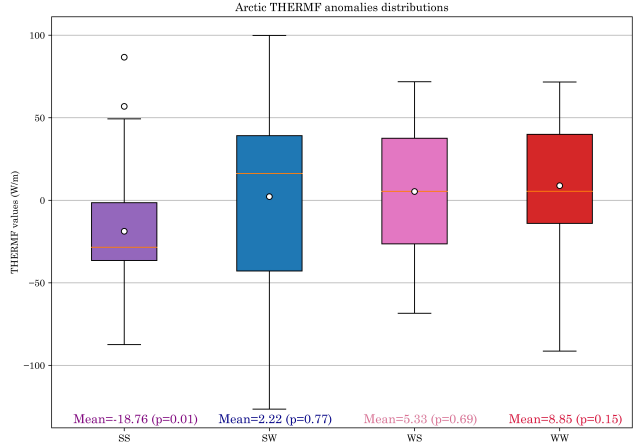


Figure 5. Box plot of the THERMF anomalies over the Arctic region (North of 70°N). Means are highlighted in white, and their numerical values are displayed at the bottom of the figure. P-values (in parentheses) are derived from bootstrap resampling with 5000 iterations.

247 ional wind and heat transport (for both the unconventional cases) (Figure ??a,d). The
 248 Arctic spatial averages of the THERMF anomalies are not significantly different from
 249 zero for both latter cases.
 250 Focusing on the THERMF anomalies of the different cases, we note that they increase
 251 from SS to SW, WS and WW (Figure 5). Specifically, conventional cases with a strong
 252 (weak) AMG-HF index show net convergence (divergence), on average, in the Arctic. For
 253 WS, a nearly-zero anomaly value is linked with the fact that blocking co-occurrence in
 254 multiple high-latitude areas effectively inhibits meridional energy transport from the lower
 255 latitudes.

256 **4 Discussion and Conclusions**

257 In this study, we analysed the relationship between Ural Blocking and the Arctic-
 258 Midlatitude thermal gradient. We found that Ural Blocking positively correlates with
 259 the AMG on interannual timescales. Specifically, when Ural Blocking is suppressed, we
 260 observe negative geopotential height anomalies over the Arctic and Siberia and positive
 261 anomalies in the midlatitudes. This is associated with an anomalous cyclonic circula-
 262 tion over the Ural region and reduced advection of midlatitude air to the Arctic, result-
 263 ing in a colder Arctic, a warmer Eurasia, and an anomalously large meridional temper-
 264 ature gradient. Conversely, when Ural Blocking is enhanced, there are positive Z500 anoma-
 265 lies over Siberia and negative anomalies further South, an anticyclonic circulation anomaly
 266 over the Urals, and enhanced advection of midlatitude airmasses towards the Arctic. This
 267 results in an anomalously warm Eurasian Arctic, and an anomalously cold Eurasia. These
 268 findings are in line with the known role of Ural blocking in modulating Arctic temper-
 269 atures and sea-ice cover, and with the Warm Arctic - Cold Eurasia pattern which has
 270 been amply discussed in the literature (D. Luo, Xiao, Yao, et al., 2016; D. Luo, Xiao,
 271 Diao, et al., 2016; Tyrllis et al., 2020; Ye & Messori, 2020).
 272 However, the linear correlation between Ural Blocking and the meridional temperature
 273 gradient only explains a small amount of the shared variability, indicating that a more
 274 complex relationship is in place. Therefore, we explored the Ural Blocking – Arctic-Midlatitude
 275 thermal gradient connection focusing on the situations characterised by intense Ural block-
 276 ing activity and strong gradient, and viceversa. When reduced Ural blocking activity is
 277 accompanied by a weaker gradient, we show that the reduced blocking is actually the
 278 consequence of a northward shift of the blocking area, from the Ural region to the Barents-

279 Kara seas. This is associated with positive Z500 anomalies over the Arctic basin, and
 280 a spatially extended positive temperature anomaly in the Arctic ocean. Eurasian cold
 281 temperature anomalies are relatively weak, suggesting that the warm anomalies in the
 282 Arctic, associated with the blocking displacement, are the main drivers of the reduced
 283 meridional temperature gradient. On the other hand, when intense Ural Blocking is ac-
 284 companied by a stronger gradient, we observe blocking developing more frequently than
 285 climatology over Greenland and close to the Bering Strait region, hindering poleward
 286 advection of midlatitude airmasses and resulting in a colder than usual Arctic. Associ-
 287 ated with the concomitant occurrence of Ural, Greenland and Bering Strait region block-
 288 ing, widespread anomalies are observed over northern Africa. These may originate from
 289 the interplay between the blocking anomalies and jet dynamics or hemispheric Rossby-
 290 wave patterns. Again, the Arctic anomalies appear as the main drivers of the anomalous
 291 meridional temperature gradient.
 292 Our results show that the documented relationship between UB and Arctic thermal anoma-
 293 lies can be modulated by modifications in the large-scale circulation in the NH at the
 294 interannual time scale. In particular, a displacement of the Ural Blocking area or the con-
 295 comitant occurrence of blocking over Greenland and the Bering Strait may drive warm
 296 or cold anomalies in the Arctic, respectively.
 297 Ultimately, our analysis can be useful for a better comprehension of the relationship be-
 298 tween Ural Blocking and other mid-high latitude climate features already investigated
 299 in literature, such as Arctic sea ice and Barents-Kara Seas atmospheric dynamics (Ruggieri
 300 et al., 2016, 2017; Chen et al., 2018; Ahmadi & Alizadeh, 2023), the stratospheric polar
 301 vortex (Peings, 2019; Tyrlis et al., 2019), and atmospheric variability modes such as
 302 North Atlantic Oscillation (B. Luo et al., 2021; Ahmadi & Alizadeh, 2023; Peings et al.,
 303 2023).

304 5 Data Availability Statement

305 All underlying ERA5 reanalysis datasets are publicly available from the Coperni-
 306 cus Climate Data Store: <https://cds.climate.copernicus.eu/cdsapp#!/home>.
 307 Python scripts implemented for this work are available upon request.

308 Acknowledgments

309 This paper and related research have been conducted during and with the support of the
 310 Italian inter-university PhD course in sustainable development and climate change (link:
 311 www.phd-sdc.it).
 312 MG acknowledge the support of the project “Dipartimento di Eccellenza 2023–2027”,
 313 funded by the Italian Ministry of Education, University and Research at IUSS Pavia.
 314 GM has received funding from the European Union’s H2020 research and innovation pro-
 315 gramme under ERC grant no. 948309 (CENÆ project).
 316 SB acknowledges partial support from the National Recovery and Resilience Plan (NRRP),
 317 Mission 4 Component 2 Investment 1.4 - Call for tender No. 1031 of 17/06/2022 of Ital-
 318 ian Ministry for University and Research funded by the European Union – NextGener-
 319 ationEU (proj. nr. CN_00000013)

320 References

- 321 Ahmadi, R., & Alizadeh, O. (2023, 8). The possible links between the barents-kara
 322 sea-ice area, ural blocking, and the north atlantic oscillation. *Quarterly Jour-*
 323 *nal of the Royal Meteorological Society*. doi: 10.1002/qj.4560
 324 AMS, American Meteorological Society. (2012). *Blocking*. Retrieved from [https://](https://glossary.ametsoc.org/wiki/Blocking)
 325 glossary.ametsoc.org/wiki/Blocking
 326 Chen, X., Luo, D., Feldstein, S. B., & Lee, S. (2018, 3). Impact of winter ural block-
 327 ing on arctic sea ice: Short-time variability. *Journal of Climate*, *31*, 2267-2282.

- 328 doi: 10.1175/JCLI-D-17-0194.1
- 329 Cho, D.-J., & Kim, K.-Y. (2021, 3). Role of ural blocking in arctic sea ice loss
330 and its connection with arctic warming in winter. *Climate Dynamics*, *56*,
331 1571-1588. doi: 10.1007/s00382-020-05545-3
- 332 Croci-Maspoli, M., Schwierz, C., & Davies, H. C. (2007, 2). A multifaceted clima-
333 tology of atmospheric blocking and its recent linear trend. *Journal of Climate*,
334 *20*, 633-649. doi: 10.1175/JCLI4029.1
- 335 Davini, P., Cagnazzo, C., Gualdi, S., & Navarra, A. (2012, 10). Bidimensional diag-
336 nostics, variability, and trends of northern hemisphere blocking. *Journal of Cli-*
337 *mate*, *25*, 6496-6509. doi: 10.1175/JCLI-D-12-00032.1
- 338 Davini, P., & D'Andrea, F. (2020, 12). From cmip3 to cmip6: Northern hemisphere
339 atmospheric blocking simulation in present and future climate. *Journal of Cli-*
340 *mate*, *33*, 10021-10038. doi: 10.1175/JCLI-D-19-0862.1
- 341 Davini, P., Weisheimer, A., Balmaseda, M., Johnson, S. J., Molteni, F., Roberts,
342 C. D., ... Stockdale, T. N. (2021, 1). The representation of winter north-
343 ern hemisphere atmospheric blocking in ecmwf seasonal prediction systems.
344 *Quarterly Journal of the Royal Meteorological Society*, *147*, 1344-1363. doi:
345 10.1002/qj.3974
- 346 Davy, R., Chen, L., & Hanna, E. (2018, 10). Arctic amplification metrics. *Internat-*
347 *ional Journal of Climatology*, *38*, 4384-4394. doi: 10.1002/joc.5675
- 348 Deser, C., Tomas, R. A., & Sun, L. (2015, 3). The role of ocean-atmosphere cou-
349 pling in the zonal-mean atmospheric response to arctic sea ice loss. *Journal of*
350 *Climate*, *28*, 2168-2186. doi: 10.1175/JCLI-D-14-00325.1
- 351 England, M. R., Eisenman, I., Lutsko, N. J., & Wagner, T. J. W. (2021, 8). The re-
352 cent emergence of arctic amplification. *Geophysical Research Letters*, *48*. doi:
353 10.1029/2021GL094086
- 354 Francis, J. A., & Vavrus, S. J. (2015, 1). Evidence for a wavier jet stream in re-
355 sponse to rapid arctic warming. *Environmental Research Letters*, *10*, 014005.
356 doi: 10.1088/1748-9326/10/1/014005
- 357 Graversen, R. G., & Burtu, M. (2016, 7). Arctic amplification enhanced by la-
358 tent energy transport of atmospheric planetary waves. *Quarterly Journal of the*
359 *Royal Meteorological Society*, *142*, 2046-2054. doi: 10.1002/qj.2802
- 360 Hersbach, H., Bell, B., Berrisford, P., Hirahara, S., Horányi, A., Muñoz-Sabater, J.,
361 ... Thépaut, J. (2020, 7). The era5 global reanalysis. *Quarterly Journal of the*
362 *Royal Meteorological Society*, *146*, 1999-2049. doi: 10.1002/qj.3803
- 363 Hwang, J., Son, S.-W., Martineau, P., & Barriopedro, D. (2022, 10). Impact of
364 winter blocking on surface air temperature in east asia: Ural versus okhotsk
365 blocking. *Climate Dynamics*, *59*, 2197-2212. doi: 10.1007/s00382-022-06204-5
- 366 Kautz, L.-A., Martius, O., Pfahl, S., Pinto, J. G., Ramos, A. M., Sousa, P. M., &
367 Woollings, T. (2022, 3). Atmospheric blocking and weather extremes over the
368 euro-atlantic sector – a review. *Weather and Climate Dynamics*, *3*, 305-336.
369 doi: 10.5194/wcd-3-305-2022
- 370 Kim, S.-H., Sung, H.-J., Kim, S.-J., Baek, E.-H., Moon, J.-Y., & Kim, B.-M. (2022,
371 7). Contribution of ural and kamchatka blockings to the amplified warm arctic-
372 cold eurasia pattern under arctic sea ice loss and eurasian cooling. *Journal*
373 *of Climate*, *35*, 4071-4083. doi: 10.1175/JCLI-D-21-0635.1
- 374 Kroese, D. P., Brereton, T., Taimre, T., & Botev, Z. I. (2014, 11). Why the monte
375 carlo method is so important today. *WIREs Computational Statistics*, *6*, 386-
376 392. doi: 10.1002/wics.1314
- 377 Kwon, Y.-O., Seo, H., Ummenhofer, C. C., & Joyce, T. M. (2020, 2). Impact of mul-
378 tidecadal variability in atlantic sst on winter atmospheric blocking. *Journal of*
379 *Climate*, *33*, 867-892. doi: 10.1175/JCLI-D-19-0324.1
- 380 Luo, B., Luo, D., Dai, A., Simmonds, I., & Wu, L. (2021, 9). A connection of winter
381 eurasian cold anomaly to the modulation of ural blocking by enso. *Geophysical*
382 *Research Letters*, *48*. doi: 10.1029/2021GL094304

- 383 Luo, D., Xiao, Y., Diao, Y., Dai, A., Franzke, C. L. E., & Simmonds, I. (2016, 6).
 384 Impact of ural blocking on winter warm arctic–cold eurasian anomalies. part ii:
 385 The link to the north atlantic oscillation. *Journal of Climate*, *29*, 3949-3971.
 386 doi: 10.1175/JCLI-D-15-0612.1
- 387 Luo, D., Xiao, Y., Yao, Y., Dai, A., Simmonds, I., & Franzke, C. L. E. (2016, 6).
 388 Impact of ural blocking on winter warm arctic–cold eurasian anomalies. part
 389 i: Blocking-induced amplification. *Journal of Climate*, *29*, 3925-3947. doi:
 390 10.1175/JCLI-D-15-0611.1
- 391 Luo, D., Yao, Y., Dai, A., Simmonds, I., & Zhong, L. (2017, 5). Increased quasi
 392 stationarity and persistence of winter ural blocking and eurasian extreme cold
 393 events in response to arctic warming. part ii: A theoretical explanation. *Jour-
 394 nal of Climate*, *30*, 3569-3587. doi: 10.1175/JCLI-D-16-0262.1
- 395 Papritz, L. (2020, 2). Arctic lower-tropospheric warm and cold extremes: Horizontal
 396 and vertical transport, diabatic processes, and linkage to synoptic circulation
 397 features. *Journal of Climate*, *33*, 993-1016. doi: 10.1175/JCLI-D-19-0638.1
- 398 Peings, Y. (2019, 5). Ural blocking as a driver of early-winter stratospheric
 399 warmings. *Geophysical Research Letters*, *46*, 5460-5468. doi: 10.1029/
 400 2019GL082097
- 401 Peings, Y., Davini, P., & Magnusdottir, G. (2023, 3). Impact of ural block-
 402 ing on early winter climate variability under different barents-kara sea ice
 403 conditions. *Journal of Geophysical Research: Atmospheres*, *128*. doi:
 404 10.1029/2022JD036994
- 405 Previdi, M., Smith, K. L., & Polvani, L. M. (2021, 9). Arctic amplification of cli-
 406 mate change: a review of underlying mechanisms. *Environmental Research Let-
 407 ters*, *16*, 093003. doi: 10.1088/1748-9326/ac1c29
- 408 Ruggieri, P., Buizza, R., & Visconti, G. (2016, 5). On the link between barents-kara
 409 sea ice variability and european blocking. *Journal of Geophysical Research: At-
 410 mospheres*, *121*, 5664-5679. doi: 10.1002/2015JD024021
- 411 Ruggieri, P., Kucharski, F., Buizza, R., & Ambaum, M. H. P. (2017, 4). The tran-
 412 sient atmospheric response to a reduction of sea-ice cover in the barents and
 413 kara seas. *Quarterly Journal of the Royal Meteorological Society*, *143*, 1632-
 414 1640. doi: 10.1002/qj.3034
- 415 Scherrer, S. C., Croci-Maspoli, M., Schwierz, C., & Appenzeller, C. (2005, 2). Two-
 416 dimensional indices of atmospheric blocking and their statistical relationship
 417 with winter climate patterns in the euro-atlantic region. *International Journal
 418 of Climatology*, *26*, 233-249. doi: 10.1002/joc.1250
- 419 Screen, J. A., & Francis, J. A. (2016, 9). Contribution of sea-ice loss to arctic am-
 420 plification is regulated by pacific ocean decadal variability. *Nature Climate
 421 Change*, *6*, 856-860. doi: 10.1038/nclimate3011
- 422 Screen, J. A., & Simmonds, I. (2010, 4). The central role of diminishing sea ice in re-
 423 cent arctic temperature amplification. *Nature*, *464*, 1334-1337. doi: 10.1038/
 424 nature09051
- 425 Shaw, T. A., Baldwin, M., Barnes, E. A., Caballero, R., Garfinkel, C. I., Hwang, Y.-
 426 T., . . . Voigt, A. (2016, 9). Storm track processes and the opposing influences
 427 of climate change. *Nature Geoscience*, *9*, 656-664. doi: 10.1038/ngeo2783
- 428 Tibaldi, S., & Molteni, F. (1990). On the operational predictability of blocking. *Tel-
 429 lus A*, *42*, 343-365. doi: 10.1034/j.1600-0870.1990.t01-2-00003.x
- 430 Tyrlis, E., Bader, J., Manzini, E., & Matei, D. (2021, 1). Reconciling different meth-
 431 ods of high-latitude blocking detection. *Quarterly Journal of the Royal Mete-
 432 orological Society*, *147*, 1070-1096. Retrieved from [https://onlinelibrary
 433 .wiley.com/doi/10.1002/qj.3960](https://onlinelibrary.wiley.com/doi/10.1002/qj.3960) doi: 10.1002/qj.3960
- 434 Tyrlis, E., Bader, J., Manzini, E., Ukita, J., Nakamura, H., & Matei, D. (2020, 7).
 435 On the role of ural blocking in driving the warm arctic–cold siberia pattern.
 436 *Quarterly Journal of the Royal Meteorological Society*, *146*, 2138-2153. doi:
 437 10.1002/qj.3784

- 438 Tyrlis, E., Manzini, E., Bader, J., Ukita, J., Nakamura, H., & Matei, D. (2019,
439 11). Ural blocking driving extreme arctic sea ice loss, cold eurasia, and
440 stratospheric vortex weakening in autumn and early winter 2016–2017.
441 *Journal of Geophysical Research: Atmospheres*, *124*, 11313–11329. doi:
442 10.1029/2019JD031085
- 443 Wazneh, H., Gachon, P., Laprise, R., de Vernal, A., & Tremblay, B. (2021, 4). At-
444 mospheric blocking events in the north atlantic: trends and links to climate
445 anomalies and teleconnections. *Climate Dynamics*, *56*, 2199–2221. Retrieved
446 from <https://link.springer.com/10.1007/s00382-020-05583-x> doi:
447 10.1007/s00382-020-05583-x
- 448 Woollings, T., Barriopedro, D., Methven, J., Son, S. W., Martius, O., Harvey, B., ...
449 Seneviratne, S. (2018). Blocking and its response to climate change. *Current*
450 *Climate Change Reports*, *4*, 287–300. doi: 10.1007/s40641-018-0108-z
- 451 Yao, Y., Luo, D., Dai, A., & Simmonds, I. (2017a, 5). Increased quasi stationarity
452 and persistence of winter ural blocking and eurasian extreme cold events in re-
453 sponse to arctic warming. part i: Insights from observational analyses. *Journal*
454 *of Climate*, *30*, 3549–3568. doi: 10.1175/JCLI-D-16-0261.1
- 455 Yao, Y., Luo, D., Dai, A., & Simmonds, I. (2017b, 5). Increased quasi stationarity
456 and persistence of winter ural blocking and eurasian extreme cold events in re-
457 sponse to arctic warming. part i: Insights from observational analyses. *Journal*
458 *of Climate*, *30*, 3549–3568. doi: 10.1175/JCLI-D-16-0261.1
- 459 Ye, K., & Messori, G. (2020, 7). Two leading modes of wintertime atmospheric cir-
460 culation drive the recent warm arctic–cold eurasia temperature pattern. *Jour-
461 nal of Climate*, *33*, 5565–5587. doi: 10.1175/JCLI-D-19-0403.1